# Study of Frisbee Flight and Rebound Dynamics Based on Frame Conversion and Vector Transformation

Bowei Yang

Beijing National Day School Beijing, China

bowie-yang@qq.com

**Abstract.** Frisbee is a kind of sports equipment in an airfoil shape that can glide in the air for throw and catch. The Frisbee-like unmanned aerial vehicles have potential as the next generation aircraft. This paper is the first one to investigate the touchdown dynamics of the Frisbee to the best of the author's knowledge. The numerical simulation of Frisbee is developed based on rigid body dynamics and aerodynamic database from existing experiments. The moment of inertia of Frisbee is determined using the three-wire pendulum method. The Frisbee is launched by a launcher and the motion is recorded by two cameras. A frame-by-frame analysis of recorded flight video using the software tracker provides the linear velocities, position, and other dynamic parameters before and after touchdown. A comparison between experimental measurement and numerical simulation results is done. The results demonstrate that the established model captures the influence of aerodynamic forces and self-spinning of Frisbee during flight and rebound. The future directions that this research might be extended and applied are discussed.

**Keywords:** Frisbee, Rebound, Rigid body dynamics, Attitude dynamics.

## 1. Introduction

Generally speaking, Frisbee (also known as a flying disc) refers to a type of aircraft-like sports equipment. It is aerodynamically designed and obtains stability by spinning during flight. When throwing Frisbee toward the ground, sometimes, Frisbee will rebound and glide for some distances before falling to the ground. Minor rebound could also be observed during Frisbee's landing after a flight.

The study of the Frisbee landing has certain potential application prospects. Frisbee gains stability the way similar to many innovative types of aerial manned and unmanned vehicles. Method to study the landing and rebound process of Frisbee can be applied to the landing of many similar self-stabilized aircraft. As an example, a disc-wing aircraft prototype called the Avrocar is proposed in the 1950s. The lift is generated through a giant torborotor located at its center, and the torborotor also provides gyroscopic action to the aircraft[5]. Another example is the Turboplan, a radio-controlled toy sold in the early 1980s. The Turboplan shares more similarities with Frisbee than Avrocar. The rotor at the center provides lift and stability, and a rotating ring surrounding the rotor also provides a large portion of the stability [5]. In addition, Frisbee-like unmanned aerial vehicle has advantages over the conventional unmanned aerial vehicles. Frisbee's low-aspect-ratio wing potentially have high performance at low speed and a high attack angle [5]. Also, the symmetric shape and the elegant design means that it is easier to carry compared with other complex UAV, which can suffer severe damage during packaging [5]. These characteristics of Frisbee suggest the prospect that a novel unmanned aerial vehicle could be designed based on the dynamics of Frisbee, and study over the landing process can provide insights for the design.

G. D. Stilley and D. L. Carstens studied the application of Frisbee flight principle on special deliveries [3]. The kinematic and aerodynamic parameters of Frisbee have been analyzed by numerically solving dynamic differential equations simplified at different levels. One paper explained the flight mechanics of Frisbee qualitatively including imposed aerodynamic forces and moments [1]. M. Hubbard and S. A. Hummel provided a model using the Euler angle to calculate the forces exerted on Frisbee in 2000. The aerodynamic coefficients were provided as a simplified fitting function [10]. In 2005, V. R. Morrison provided a simplified 2-dimensional model of Frisbee flight. Equations for

the aerodynamic forces in this study is based on hydromechanics [16]. In 2010, K. Baumback provided an extension to the model suggested by V. R. Morrison and described Frisbee's 3-dimensional motion using program simulation [11]. In 2019, one research was conducted, focusing on explaining Frisbee's flight using Newton's second law [14].

Several other studies focused on measuring the aerodynamic parameters of Frisbee using different methods. Using a MEMS triaxial gyroscope, Y. Weizman measured the angular velocity, the aerodynamic torque, and the decay of spin rate of Frisbee during flight [18]. A new method of identifying Frisbee's aerodynamic coefficients by real flight data was suggested by S. A. Hummel and M. Hubbard. This new method could be used as an alternative to wind tunnel tests [9]. Frisbee aerodynamic coefficients are obtained in wind tunnel tests by J. R. Potts and W. J. Crowther. [4]. In 1999, K. Yasuda recorded the trajectory of Frisbee during free flight using two sets of cameras. By analyzing the videos, the frequency of occurrence of different initial parameters when Frisbee is thrown by hand is determined [12]. A comprehensive study over aerodynamic characteristics of flying dynamic of golf disc with different thickness, cavity, and edge shapes was reported using wind tunnel experiments [13]. Additionally, a Frisbee launching robot was built according to the flying principle of Frisbee. The robot can automatically control the initial parameters such as velocity and pitch angle of Frisbee [17].

The landing process of Frisbee is quite similar to the process of stone skipping, involve the process of a spinning object impact with a certain surface and rebound. There are two highly renowned research papers that investigated the dynamic of stone skipping, and determined a "magic angle" of impact to maximize the numbers of times of skipping both theoretically [7] and experimentally [8]. By mimic the process of stone skipping, the British army successfully designed a bouncing bomb during World War II to take down damps. [5].

This work established a theoretical model used to calculate the rebound process. The model takes friction, the impulse from the ground, and different aerodynamic forces into consideration. A damping harmonic motion model is used to describe the impact. MATLAB simulation is performed based on the dynamic differential equation derived. Several sets of experiments were conducted with different initial launching parameters. The experimental data is compared with the simulation result to verify the proposed theoretical model.

## 2. Theoretical Model of Frisbee Flight

### 2.1. Forces during flight

Complete wind tunnel experiment was conducted to determine the three aerodynamic parameter, lift coefficient, drag coefficient, and pitching moment coefficient, of standard Frisbee in 2002 [4], and the data of the conducted experiment is presented in three figures in another research paper crafted by the same authors in 2007 [15, Figure 3].

#### 2.1.1 Lift force

Lift force results from Frisbee's wing shaped cross section. The lift force could be calculated using equation (1).

$$F_L = \frac{1}{2}\rho v^2 S C_L \tag{1}$$

In the equation, $S$ is the area of the surface of the airfoil. In this case, is the area of Frisbee, which is 0.05726m$^2$. $C_L$ is the lift coefficient of Frisbee, $\rho$ is the density of air and $v$ is the instantaneous linear velocity.

The variation of lift coefficient as a function of attack angle is presented in Figure 1. The original data is extrapolated from the range of -0.2$rad$ to 0.6$rad$ to the range of -1$rad$ to 1$rad$.

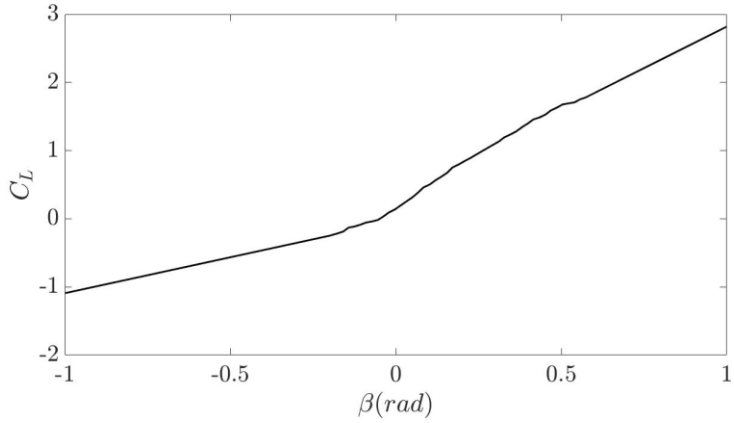


**Figure 1.** data of lift coefficient, extrapolated from the range of -0.2$rad$ to 0.6$rad$ to the range of -1$rad$ to 1$rad$.

### 2.1.2 Drag Force

The drag force of Frisbee could be calculated using equation (2):

$$F_D = \frac{1}{2}\rho v^2 S C_D \tag{2}$$

Experiment data of drag coefficient, which also varies as a function of the attack angle, is presented in Figure 2. The original data is extrapolated from the range of -0.2$rad$ to 0.6$rad$ to the range of -1$rad$ to 1$rad$.

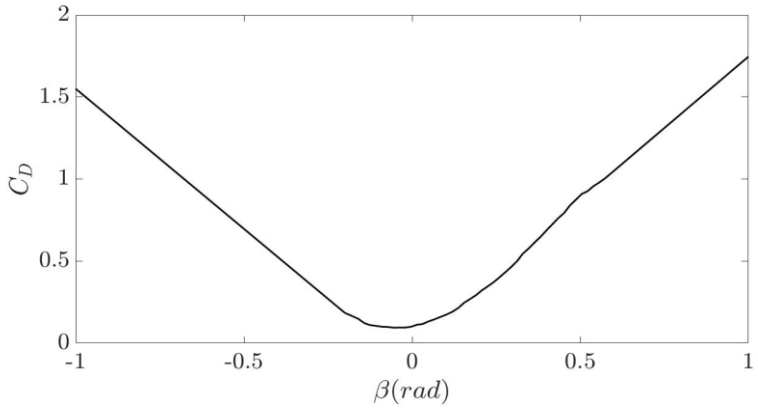


**Figure 2.** data of drag coefficient, extrapolated from the range of -0.2$rad$ to 0.6$rad$ to the range of -1$rad$ to 1$rad$.

## 2.2. Moment

### 2.2.1 Pitching moment

With the action point of the lift force moving forward, a torque is exerted on Frisbee. The pitching moment could be calculated using equation 3.

$$\tau_p = \frac{1}{2}\rho v^2 S d C_M \tag{3}$$

In the equation, $\tau_p$ is the pitching torque action on the Frisbee, and$d$ is the diameter of Frisbee, $C_M$ is the pitching moment coefficient.

Experiment data of the pitching moment coefficient as a function of the attack angle from past research [4] is presented in Figure 3. The original data is extrapolated from the range of -0.2$rad$ to 0.6$rad$ to the range of -1$rad$ to 1$rad$.

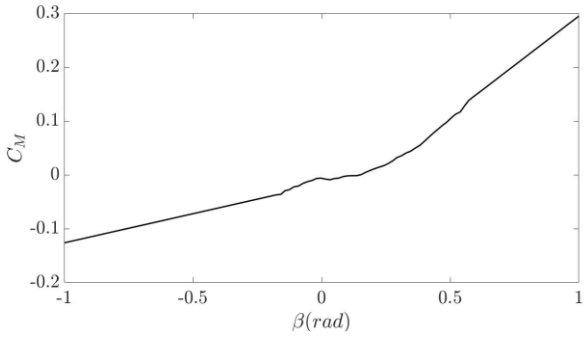


(a)

**Figure 3.** data of pitching moment coefficient, extrapolated from the range of -0.2$rad$ to 0.6$rad$ to the range of -1$rad$ to 1$rad$.

### 2.3. Frame conversion of forces and moments

Four frames will be used to calculate motion, the inertial frame, Frisbee's embedded reference frame, the sideslip frame, and the velocity vector frame. This system of convert and unify vectors is first proposed by W. J. Crowther and J. R. Potts [15]. Definition for the frames are presented below.

#### 2.3.1 Definition of four frames

The inertial frame has $x$ and $y$ axis lying on the surface of ground and $z$ axis perpendicular to ground, assuming that the ground is perfectly horizontal. The embedded reference frame has the origin set at the center of mass of Frisbee, $x'$ and $y'$ axis lying horizontally on the plane formed by the Frisbee's upper surface, and $z'$ perpendicular to the surface of Frisbee. Originally, the $x$ axis point toward the direction of motion, as the Frisbee rotates, the embedded frame rotate along with Frisbee around $z'$ axis.

The sideslip frame $x''y''z''$ is obtained by rotating the embedded frame with respect to the $z'$ axis so that the $x''$ axis align with the direction of the projection of velocity on the $x'y'$ plane. The velocity vector frame $x'''y'''z'''$ is then obtained by rotating sideslip frame along $y''$ axis so that the $x'''$ axis align with the velocity vector. The angle which distinct the embedded frame from sideslip frame is the sideslip angle $\alpha$; the angle distinct the sideslip frame from velocity vector frame is the attack angle $\beta$. Sketch of the four frames are presented in Figure 4.

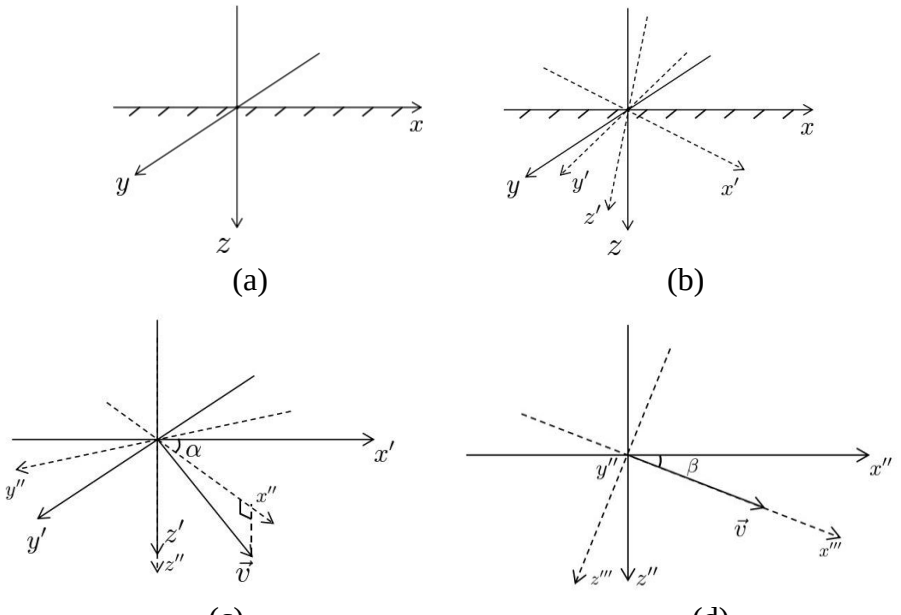


**Figure 4.** Illustration of the four frames and the relationship between them. (a): Inertial frame; (b): Embedded frame; (c): Sideslip frame; (d): Velocity vector frame.

### 2.3.2 Euler angles

The rotation sequence used in this research is the $zyx$ sequence, breaking the orientation down into rotation around $z$, $y$ and $x$ axis in succession. The Euler angles in this convention are commonly known as the yaw, pitch and row angle, labeled $\phi$, $\theta$ and $\psi$ respectively. In order to describe the attitude of Frisbee relative to the ground, a rotational matrix in terms of Euler angles is defined to transform inertial frame into the embedded frame.

$$T_{i2e} = \begin{bmatrix} 1 & 0 & 0 \\ 0 & \cos\phi & \sin\phi \\ 0 & -\sin\phi & \cos\phi \end{bmatrix}$$

$$\begin{bmatrix} \cos\theta & 0 & -\sin\theta \\ 0 & 1 & 0 \\ \sin\theta & 0 & \cos\theta \end{bmatrix} \begin{bmatrix} \cos\psi & \sin\psi & 0 \\ -\sin\psi & \cos\psi & 0 \\ 0 & 0 & 1 \end{bmatrix} \tag{4}$$

The Euler angles are time dependent variables, and their derivatives are related to the angular velocity of Frisbee in the embedded frame, which has components $p$, $q$, and $r$, by equation (5) [2].

$$\begin{bmatrix} \dot{\phi} \\ \dot{\theta} \\ \dot{\psi} \end{bmatrix} = \frac{1}{\cos\theta} \begin{bmatrix} \cos\theta & \sin\phi\sin\theta & \cos\phi\sin\theta \\ 0 & \cos\phi\cos\theta & -\sin\phi\cos\theta \\ 0 & \sin\phi & \cos\phi \end{bmatrix} \begin{bmatrix} p \\ q \\ r \end{bmatrix} \tag{5}$$

### 2.3.3 Converting forces into inertial frame

Based on the definition, the lift force points toward the negative $z'''$ axis in velocity vector frame, perpendicular to the direction of speed and the $y'''$ axis, while drag force points toward negative $x'''$ axis in velocity vector frame. The pitching moment points toward positive $y'''$ axis in velocity vector frame. The aerodynamic forces and moment could all be transformed into the inertial frame by multiplying several rotational matrices. The rotational matrix transforming embedded frame to sideslip frame is presented by equation (6), and the rotational matrix for transforming sideslip frame to velocity vector frame is presented in equation (7).

$$T_{e2s} = \begin{bmatrix} \cos\alpha & \sin\alpha & 0 \\ -\sin\alpha & \cos\alpha & 0 \\ 0 & 0 & 1 \end{bmatrix} \tag{6}$$

$$T_{s2v} = \begin{bmatrix} \cos\beta & 0 & \sin\beta \\ 0 & 1 & 0 \\ -\sin\beta & 0 & \cos\beta \end{bmatrix} \tag{7}$$

Cosine and sine of the two angles could be calculated by following equation (8), (9), (10) and (11).

$$\cos\alpha = \frac{v_{x'}}{\sqrt{v_{x'}^2 + v_{y'}^2}} \tag{8}$$

$$\sin\alpha = \frac{v_{y'}}{\sqrt{v_{x'}^2 + v_{y'}^2}} \tag{9}$$

$$\cos\beta = \frac{v_{x''}}{\sqrt{v_{x''}^2 + v_{z''}^2}} \tag{10}$$

$$\sin\beta = \frac{v_{z''}}{\sqrt{v_{x''}^2 + v_{z''}^2}} \tag{11}$$

The property of rotational matrix indicates that a reverse transformation is described by the transpose of the original rotational matrix. Therefore, the reverse rotational matrix from velocity vector

frame to sideslip frame and from sideslip frame to embedded frame is obtained as equation (12) and (13).

$$T_{s2e} = T_{e2s}^{T} \tag{12}$$

$$T_{v2s} = T_{s2v}^{T} \tag{13}$$

### 2.4. Newton's second law

The linear motion of Frisbee is calculated by the differential form of Newton's second law in inertial frame:

$$m\begin{bmatrix} \dot{v_x} \\ \dot{v_y} \\ \dot{v_z} \end{bmatrix} = \begin{bmatrix} F_x \\ F_y \\ F_z \end{bmatrix} \tag{14}$$

### 2.5. Angular Momentum Theorem

The angular momentum of an object can be calculated as follows:

$$\begin{bmatrix} L_x \\ L_y \\ L_z \end{bmatrix} = \begin{bmatrix} I_x & 0 & 0 \\ 0 & I_y & 0 \\ 0 & 0 & I_z \end{bmatrix} \begin{bmatrix} \omega_x \\ \omega_y \\ \omega_z \end{bmatrix} \tag{15}$$

Torque can be related with angular acceleration $\dot{\omega}$ by the following equation:

$$\vec{\tau} = I\dot{\vec{\omega}} = \frac{d\vec{L}}{dt} \tag{16}$$

From equation of Coriolis [20], we have:

$$\overrightarrow{\tau_e} = \frac{d\overrightarrow{L_e}}{dt} + \overrightarrow{\omega_e} \times \vec{L} \tag{17}$$

Substitute $\vec{L}$ with equation (15), and arrange the equation in matrix form, we have:

$$\begin{bmatrix} \tau_{x'} \\ \tau_{y'} \\ \tau_{z'} \end{bmatrix} = \begin{bmatrix} I_x & 0 & 0 \\ 0 & I_y & 0 \\ 0 & 0 & I_z \end{bmatrix} \begin{bmatrix} \dot{p} \\ \dot{q} \\ \dot{r} \end{bmatrix} + \begin{bmatrix} 0 & -r & q \\ r & 0 & -p \\ -q & p & 0 \end{bmatrix} \begin{bmatrix} L_{x'} \\ L_{y'} \\ L_{z'} \end{bmatrix} \tag{18}$$

Therefore, the derivative of angular velocity in embedded frame $\omega_e$ is:

$$\begin{bmatrix} \dot{p} \\ \dot{q} \\ \dot{r} \end{bmatrix} = \begin{bmatrix} I_x & 0 & 0 \\ 0 & I_y & 0 \\ 0 & 0 & I_z \end{bmatrix}^{-1} \begin{bmatrix} \tau_{x'} \\ \tau_{y'} \\ \tau_{z'} \end{bmatrix} - \begin{bmatrix} I_x & 0 & 0 \\ 0 & I_y & 0 \\ 0 & 0 & I_z \end{bmatrix}^{-1} \begin{bmatrix} 0 & -r & q \\ r & 0 & -p \\ -q & p & 0 \end{bmatrix} \begin{bmatrix} L_{x'} \\ L_{y'} \\ L_{z'} \end{bmatrix} \tag{19}$$

### 2.6. Dynamic Differential Equation

#### 2.6.1 Position

The position could be calculated using dynamic differential equation in matrix form:

$$\begin{bmatrix} \dot{x} \\ \dot{y} \\ \dot{z} \end{bmatrix} = \begin{bmatrix} v_x \\ v_y \\ v_z \end{bmatrix} \tag{20}$$

### 2.6.2 Linear velocity

Define an aerodynamic coefficient matrix in velocity vector frame:

$$C_a = \begin{bmatrix} -C_D \\ 0 \\ -C_L \end{bmatrix} \tag{21}$$

which gives us the magnitude and direction of the aerodynamic forces. The aerodynamic forces could therefore be determined in velocity vector frame as:

$$F_{va} = \frac{1}{2}\rho v^2 S C_a \tag{22}$$

Transform the forces into the inertial frame by multiplying the transformation matrix:

$$F_{ia} = T_{g2e}^T T_{e2s}^T T_{s2v}^T F_{va} \tag{23}$$

By adding gravity to the aerodynamic force in inertial frame, the total force exerted on Frisbee during flight is determined:

$$F_{if} = F_{ia} + \begin{bmatrix} 0 \\ 0 \\ mg \end{bmatrix} \tag{24}$$

Substitute equation (24) into Newton's second law in equation (14) to calculate the acceleration, and expand the equation, we get the dynamic differential equation for the components of linear velocity in inertial frame:

$$m\dot{v}_x = \frac{1}{2}\Big(SC_D\rho\big(\cos\beta\,(\sin\alpha\,(\cos\phi\sin\psi - \cos\psi\sin\phi\sin\theta) - \cos\psi\cos\alpha\cos\theta) - \sin\beta\,(\sin\phi\sin\psi + \cos\phi\cos\psi\sin\theta)\big)\big(v_x^2 + v_y^2 + v_z^2\big)\Big) - \frac{1}{2}\Big(SC_L\rho\big(\sin\beta\,(\sin\alpha\,(\cos\phi\sin\psi - \cos\psi\sin\phi\sin\theta) - \cos\psi\cos\alpha\cos\theta) + \cos\beta\,(\sin\phi\sin\psi + \cos\phi\cos\psi\sin\theta)\big)\big(v_x^2 + v_y^2 + v_z^2\big)\Big) \tag{25}$$

$$m\dot{v}_y = -\frac{1}{2}\Big((SC_D\rho\big(\cos\beta\,(\sin\alpha\,(\cos\phi\cos\psi + \sin\phi\sin\psi\sin\theta) + \cos\alpha\cos\theta\sin\psi) - \sin\beta\,(\cos\psi\sin\phi - \cos\phi\sin\psi\sin\theta)\big)\big(v_x^2 + v_y^2 + v_z^2\big)\Big) - \frac{1}{2}\Big(SC_L\rho\big(\sin\beta\,(\sin\alpha\,(\cos\phi\cos\psi + \sin\phi\sin\psi\sin\theta) + \cos\alpha\cos\theta\sin\psi) + \cos\beta\,(\cos\psi\sin\phi - \cos\phi\sin\psi\sin\theta)\big)\big(v_x^2 + v_y^2 + v_z^2\big)\Big) \tag{26}$$

$$m\dot{v}_z = \Big(mg + \frac{1}{2}\Big(SC_D\rho(\cos\beta\,(\cos\alpha\sin\theta - \cos\theta\sin\phi\sin\alpha) - \cos\phi\sin\beta\cos\theta)\big(v_x^2 + v_y^2 + v_z^2\big)\Big) - \frac{1}{2}\Big(SC_D\rho(\sin\beta\,(\cos\alpha\sin\theta - \cos\theta\sin\phi\sin\alpha) + \cos\beta\cos\phi\cos\theta)\big(v_x^2 + v_y^2 + v_z^2\big)\Big)\Big) \tag{27}$$

### 2.6.3 Angular velocity

Similar to the aerodynamic forces Frisbee experiences, a moment coefficient matrix is also defined in velocity vector frame as:

$$C_{moment} = \begin{bmatrix} 0 \\ C_M \\ 0 \end{bmatrix} \tag{28}$$

which gives the magnitude and direction of the aerodynamic moment. The moment could then be determined in velocity vector frame:

$$\tau_{va} = \frac{1}{2}\rho v^2 S d C_{moment} \tag{29}$$

The aerodynamic torque could then be transformed into the embedded frame by multiplying the transformation matrix.

$$\tau_{ea} = T_{e2s}^T T_{s2v}^T \tau_{va} \tag{30}$$

Substitute equation (30) into equation (28) to calculate the angular acceleration, and we get the dynamic differential equation for the component of angular velocity in embedded frame:

$$I_x\dot{p} = -\left(I_z qr - I_y qr + \frac{1}{2}\left(\rho\left(v_x^2 + v_y^2 + v_z^2\right)SdC_M \sin\alpha\right)\right) \tag{31}$$

$$I_y\dot{q} = I_z pr - I_x pr + \frac{1}{2}\left(\rho\left(v_x^2 + v_y^2 + v_z^2\right)SdC_M \cos\alpha\right) \tag{32}$$

$$I_z\dot{r} = I_x pq - I_y pq = 0 \tag{33}$$

## 3. Theoretical Model of Frisbee Rebound

### 3.1. Basic model of ground

The ground is treated as a damping spring in this model. The position as a function of time [19] during damping harmonic motion is determined as follows in this specific case:

$$z = A_0 e^{\frac{-bt}{2m}} \sin\omega' t \tag{34}$$

The phase angle $\delta$ in the original equation is approximated to be $-\frac{\pi}{2}$ in this scenario. Take the first derivative of the position function to obtain velocity function:

$$v = -A_0 e^{\frac{-bt}{2m}}\left(\frac{-b}{2m}\sin\omega' t - \omega'\cos\omega' t\right) \tag{35}$$

When time $t = 0$, we have:

$$v_0 = A_0\omega' \tag{36}$$

Assuming that during rebound, Frisbee is in contact with the ground for $t_1$ seconds. At time $t = t_1$, we then have:

$$v_1 = -A_0\omega' e^{\frac{-bt_1}{2m}} \tag{37}$$

Define a coefficient of restitution $\chi$ as the initial rebound speed over the ultimate falling speed:

$$\chi = \frac{|v_1|}{v_0} = e^{\frac{-bt_1}{2m}} \tag{38}$$

The damping coefficient $b$ is obtained as:

$$b = -\frac{2m\ln\chi}{t_1} \tag{39}$$

The following equation is used to calculate the angular frequency $\omega'$ [19]:

$$\omega' = \omega_0\sqrt{1 - \left(\frac{b}{2m\omega_0}\right)^2} \tag{40}$$

Substitute $\omega_0$ into equation (53), and square both side of the equation, we have:

$$\omega'^2 = \frac{k}{m}\left(1 - \frac{m}{k}\left(\frac{b}{2m}\right)^2\right) = \frac{k}{m} - \frac{\ln^2\chi}{t_1^2} \tag{41}$$

At time $t = t_1$, we have the relationship between the angular frequency as follows:

$$\omega' = \frac{\pi}{t_1} \tag{42}$$

We therefore obtained the following equation to calculate the spring constant:

$$k = m\left(\frac{\pi^2}{t_1^2} + \frac{\ln^2\chi}{t_1^2}\right) \tag{43}$$

### 3.2. Determine Frisbee's initial attitude during rebound

#### 3.2.1 Determine the angle between Frisbee and ground

The angle between Frisbee and ground is the same as the angle between the $z'$ axis and $z$ axis. Define a unit vector $\widehat{z'}$ pointing at positive $z'$ direction in embedded frame first. Representing this unit vector in inertial frame $\widehat{z_i'}$:

$$\widehat{z_i'} = \begin{bmatrix} z_{ix}' \\ z_{iy}' \\ z_{iz}' \end{bmatrix} = C_{i2e}^T \widehat{z'} = \begin{bmatrix} \sin\phi \sin\psi + \cos\phi \cos\psi \sin\theta \\ \cos\phi \sin\psi \sin\theta - \cos\psi \sin\phi \\ \cos\phi \cos\theta \end{bmatrix} \tag{44}$$

Define another unit vector $\hat{z}$ pointing at positive $z$ axis in inertial frame. By multiplying this vector with unit vector $\widehat{z_i'}$, we have:

$$\hat{z} \cdot \widehat{z_i'} = \cos\sigma = \cos\phi \cos\theta \tag{45}$$

In the equation, $\sigma$ is the angle between $\hat{z}$ and $\widehat{z_i'}$, and is also the angle between Frisbee surface and the ground.

#### 3.2.2 Locating the point of impact with ground

The point of impact with the ground is the lowest point on the edge of Frisbee. With its location determined, we can calculate the torque on Frisbee exerted by the ground. To locate the point of contact with ground, a displacement vector $\overrightarrow{r_{pc}}$ is defined to be the position of the point of impact relative to the center of Frisbee. The location of the point of impact could then be determined by adding the displacement of Frisbee's center in space relative to origin with this vector $\overrightarrow{r_{pc}}$. The magnitude of this vector is the radius of Frisbee, $\frac{d}{2}$. The projection of this vector on the $xy$ surface is:

$$r_{xy} = \frac{d}{2}\cos\sigma \tag{46}$$

This projection is the magnitude of the vector formed by the $x$ and $y$ component of $\overrightarrow{r_{pc}}$. This component vector is in the opposite direction as the vector formed by the $x$ and $y$ component of $\widehat{z_i'}$. Normalize this formed vector of $\widehat{z_i'}$, and multiply the normalized vector with the magnitude of the component vector, the component vector could be expressed as:

$$\begin{bmatrix} r_{pcx} \\ r_{pcy} \end{bmatrix} = -\frac{r_{xy}}{\sqrt{z_{ix}'^2 + z_{iy}'^2}} \begin{bmatrix} z_{ix}' \\ z_{iy}' \end{bmatrix} \tag{47}$$

This is the $x$ and $y$ component of the displacement vector $\overrightarrow{r_{pc}}$. Because we have the angle between this vector and the ground, therefore, the $z$ component of $\overrightarrow{r_{pc}}$ could easily be calculated as:

$$r_{pcz} = \frac{d}{2}\sin\sigma = \frac{d}{2}\sqrt{1 - \cos^2\sigma} \tag{48}$$

Expand the equation for the $x$ and $y$ component, the displacement vector $\overrightarrow{r_{pc}}$ is therefore arranged in its components as:

$$\begin{bmatrix} r_{pcx} \\ r_{pcy} \\ r_{pcz} \end{bmatrix} = \frac{d}{2} \begin{bmatrix} -\frac{\cos\phi \cos\theta (\sin\phi \sin\psi + \cos\phi \cos\psi \sin\theta)}{\sqrt{1-\cos^2\sigma}} \\ \frac{\cos\phi \cos\theta (\sin\phi \cos\psi - \cos\phi \sin\psi \sin\theta)}{\sqrt{1-\cos^2\sigma}} \\ \sqrt{1 - \cos^2\sigma} \end{bmatrix} \tag{49}$$

The location of the point of contact in the inertial frame is thus:

$$r_{pci} = \begin{bmatrix} r_{xi} \\ r_{yi} \\ r_{zi} \end{bmatrix} = \begin{bmatrix} x + r_{pcx} \\ y + r_{pcy} \\ z + r_{pcz} \end{bmatrix} \tag{50}$$

In this equation, $r_{pci}$ represents the component of the displacement vector of the point of contact with respect to the origin. The velocity of this point of contact in space could then be determined by taking the derivative of $r_{pci}$:

$$v_{pci} = \dot{r}_{pci} = \begin{bmatrix} \dot{r}_{xi} \\ \dot{r}_{yi} \\ \dot{r}_{zi} \end{bmatrix} = \begin{bmatrix} v_x + \dot{r}_{pcx} \\ v_y + \dot{r}_{pcy} \\ v_z + \dot{r}_{pcz} \end{bmatrix} \tag{51}$$

The equation for the derivative of the component of $r_{pci}$ is obtained by direct calculation and used in the program.

### 3.3. Condition for touch down

This part gives the conditions under which Frisbee is considered landed and left the ground. The conditions will be used in program simulation to determine the status of rebound Frisbee. The ground is set at level in the inertial Frame. That means $y = 0$ and $x = 0$. The height, which is the $z$ component of the position of the lowest point on Frisbee is provided in equation (50). When Frisbee landed, the lowest point on Frisbee becomes lower then the ground level. The height is less or equal to 0. The vertical velocity is positive. Therefore, when the condition is as shown in equation (52), the Frisbee is considered landed.

$$\begin{cases} z + \sqrt{1 - \cos^2 \sigma} \leq 0 \\ v_z > 0 \end{cases} \tag{52}$$

Similarly, when Frisbee leaves the ground, the lowest point on Frisbee becomes higher then the ground level, and the vertical velocity is negative. The height is larger or equal to 0. Therefore, when the condition is as shown in equation (53), the Frisbee is considered left the ground.

$$\begin{cases} z + \sqrt{1 - \cos^2 \sigma} \geq 0 \\ v_z < 0 \end{cases} \tag{53}$$

### 3.4. Forces during impact

#### 3.4.1 Normal force

The normal force could be calculated using the differential equation for damper harmonic oscillation:

$$F_{zi} = -b\dot{r_{zi}} - kr_{zi} \tag{54}$$

In this equaion, $F_{zi}$ is the $z$ component of the Force exerted by the ground in inertial Frame.

#### 3.4.2 Friction

The Friction from the ground is of a determined value, and could be calculated by multiplying the normal force $F_{zi}$ with the friction coefficient of the ground:

$$F_f = \mu F_{zi} \tag{55}$$

In this equation, $\mu$ is the friction coefficient. The friction force points at a certain direction opposite to the velocity of the point of contact relative to the ground. This relative velocity lies on the $xy$ surface, and could be obtained by adding the $x$ and $y$ component of the velocity of the point of contact in space $v_{pci}$ with the tangential velocity at the point of contact due to the rotation. The magnitude of the tangential velocity is:

$$|v_t| = r\frac{d}{2} \tag{56}$$

In this equation, $v_t$ is the tangential velocity, and $r$ is the $z'$ component of Frisbee's angular velocity in the embedded frame, which is the rotational speed of Frisbee. This tangential velocity

vector is perpendicular to $\overrightarrow{r_{pc}}$, the position of the point of impact relative to the center of Frisbee, which indicates that the tangential velocity is also perpendicular to the vector $z_i'$. The direction of this tangential velocity is linked with the direction of rotation and could be calculated by Equation (57). The the tangential velocity is perpendicular to the displacement vector $\overrightarrow{r_{pc}}$.

$$v_t = sign(r)\frac{d}{2}\frac{r}{\sqrt{z_{ix}'^2+z_{iy}'^2}}\begin{bmatrix} z_{iy}' \\ -z_{ix}' \end{bmatrix} \tag{57}$$

In the equation, $sign(r)$ is a function of the sign of rotational speed $r$ defined as follows:

$$sign(r) = \begin{cases} 1 & r > 0 \\ 0 & r = 0 \\ -1 & r < 0 \end{cases} \tag{58}$$

Combining all the equations, the relative velocity of the point of contact is determined as follows:

$$v_{rel} = v_t + \begin{bmatrix} \dot{r}_{xi} \\ \dot{r}_{yi} \end{bmatrix} \tag{59}$$

The friction could thus be calculated as:

$$F_f = \begin{bmatrix} F_{fx} \\ F_{fy} \end{bmatrix} = \mu F_{iz}\frac{-v_{rel}}{|v_{rel}|} \tag{60}$$

With the forces determined, the total force exerted by ground on Frisbee could be written in its component form as:

$$F_{ig} = \begin{bmatrix} F_{fx} \\ F_{fy} \\ F_{iz} \end{bmatrix} \tag{61}$$

### 3.5. Moment during impact

The moment exerted on Frisbee by ground during impact could be calculated by taking the cross product of the force arm, which is the displacement vector $\overrightarrow{r_{pc}}$, and the force exerted by the ground, $F_{ig}$, as in equation (62). The moment could then be transformed into the embedded reference frame by multiply the moment in inertial frame with the transformation matrix $T_{i2e}$ as in equation (63).

$$\tau_{ig} = \begin{bmatrix} r_{pcx} \\ r_{pcy} \\ r_{pcz} \end{bmatrix} \times \begin{bmatrix} F_{fx} \\ F_{fy} \\ F_{iz} \end{bmatrix} \tag{62}$$

$$\tau_{eg} = T_{i2e}\tau_{ig} \tag{63}$$

In the equation, $\tau_{ig}$ is the moment from the ground, while $\tau_{eg}$ is the moment from the ground after being transformed into the embedded frame.

### 3.6. Dynamic differential equation for rebound

The dynamic differential equation for the rebound process could be determined using the same process as for flight. By adding the aerodynamic force and the impact force together, we can get the equation for the total force, and therefore could determine the differential equation for linear velocity; by adding the aerodynamic moment and the impact moment together, we can get the equation for the total moment and therefore determine the differential equation for angular velocity. Equation (64) and equation (65) describes the total force and moment respectively. The total force is represented as $F_i$, while the total moment is represented as $\tau_e$.

$$F_i = F_{if} + F_{ig} \tag{64}$$

$$\tau_e = \tau_{ea} + \tau_{eg} \tag{65}$$

The differential equation for the model considered friction is found to be too complicated. Therefore, a simplified model is used, in which the friction is neglected. The differential equations for the linear velocity at $x$ and $y$ direction as well as for angular velocity $r$ are the same as that in flight. The new differential equation for $v_z$, $p$ and $q$ is presented as equation (66), (67), and (68):

$$\begin{gathered} m\dot{v}_z = -(k(z + (d(1 - cos\,\phi^2\,cos\,\theta^2)^{\frac{1}{2}}/2) - gm \\ +(b(2v_z(1 - cos\,\phi^2\,cos\,\theta^2)^{\frac{1}{2}} + dp\,cos\,\phi\,cos\,\theta^2\,sin\,\phi \\ +dq\,cos\,\phi\,cos\,\theta\,sin\,\theta))/(2(-cos\,\phi^2\,cos\,\theta^2 + 1)^{\frac{1}{2}}) \\ +(SC_D\rho(cos\,\phi\,sin\,\beta\,cos\,\theta - cos\,\alpha\,cos\,\beta\,sin\,\theta \\ +cos\,\beta\,sin\,\alpha\,cos\,\theta\,sin\,\phi)(v_x^2 + v_y^2 + v_z^2))/2 \\ +SC_L\rho(cos\,\beta\,cos\,\phi\,cos\,\theta + cos\,\alpha\,sin\,\beta\,sin\,\theta \\ -sin\,\alpha\,sin\,\beta\,cos\,\theta\,sin\,\phi)(v_x^2 + v_y^2 + v_z^2))/2 \end{gathered} \tag{66}$$

$$\begin{gathered} I_x\dot{p} = (4I_zqr - 4I_yqr + bd^2p\,cos\,\phi^2cos\,\theta^4 \\ -bd^2p\,cos\,\phi^4\,cos\,\theta^4 + d^2k\,cos\,\phi\,cos\,\theta^2\,sin\,\phi \\ -d^2k\,cos\,\phi^3\,cos\,\theta^4\,sin\,\phi + 4I_yqr\,cos\,\phi^2cos\,\theta^2 \\ -4I_zqr\,cos\,\phi^2\,cos\,\theta^2 + 2SC_Md\rho v_x^2\,sin\,\alpha \\ +2SC_Md\rho v_y^2\,sin\,\alpha + 2SC_Md\rho v_z^2\,sin\,\alpha \\ +2bdv_z\,cos\,\phi\,cos\,\theta^2\,sin\,\phi(1 - cos\,\phi^2\,cos\,\theta^2)^{\frac{1}{2}} \\ +2dkz\,cos\,\phi\,cos\,\theta^2\,sin\,\phi(1 - cos\,\phi^2\,cos\;\theta^2)^{\frac{1}{2}} \\ +bd^2q\,cos\,\phi^2\,cos\,\theta^3\,sin\,\phi\,sin\,\theta \\ -2SC_Md\rho\,cos\,\phi^2\,sin\,\alpha\,cos\,\theta^2(v_x^2 + v_y^2 + v_z^2) \\ /(4\,cos\,\phi^2\,cos\,\theta^2 - 4) \end{gathered} \tag{67}$$

$$\begin{gathered} I_y\dot{q} = I_zpr - I_xpr + (SC_Md\rho\,cos\,\alpha(v_x^2 + v_y^2 + v_z^2))/2 \\ -(d\,cos\,\phi\,cos\,\theta(cos\,\phi\,cos\,\psi + sin\,\phi\,sin\,\psi\,sin\,\theta) \\ (sin\,\phi\,sin\,\psi + cos\,\phi\,cos\,\psi\,sin\,\theta) \\ (dk + 2(bv_z + kz)(1 - cos\,\phi^2\,cos\,\theta^2)^{\frac{1}{2}} - dk\,cos\,\phi^2\,cos\,\theta^2 \\ bdq\,cos\,\phi\,cos\,\theta\,sin\,\theta + bdp\,cos\,\phi\,cos\,\theta^2\,sin\,\phi)) \\ /(4(-cos\,\phi^2\,cos\,\theta^2 + 1)^{\frac{1}{2}}(sin\,\phi^2 + sin\,\theta^2 \\ -sin\,\phi^2\,sin\,\theta^2)^{\frac{1}{2}}) + (d\,cos\,\phi\,cos\,\theta(cos\,\phi\,sin\,\psi \\ -cos\,\psi\,sin\,\phi\,sin\,\theta)(cos\,\psi\,sin\,\phi - cos\,\phi\,sin\,\psi\,sin\,\theta) \\ (dk + 2(bv_z + kz)(1 - cos\,\phi^2\,cos\,\theta^2)^{\frac{1}{2}} \\ -dk\,cos\,\phi^2\,cos\,\theta^2 + bdq\,cos\,\phi\,cos\,\theta\,sin\,\theta \\ bdp\,cos\,\phi\,cos\,\theta^2\,sin\,\phi))/(4(-cos\,\phi^2\,cos\,\theta^2 + 1)^{\frac{1}{2}} \\ (sin\,\phi^2 + sin\,\theta^2 - sin\,\phi^2\,sin\,\theta^2)^{\frac{1}{2}}) \end{gathered} \tag{68}$$

## 4. Program Simulation

The dynamic differential equation derived in section 2 and 3 are solved using MATLAB ODE23s numerical solver, and program is coded to transfer these numerical solution into graphs containing dynamic variables such as linear velocity as a function of time. Flowcharts for the coding logic of dynamic simulation program is presented below.

### 4.1. Flowchart of the dynamic simulation program

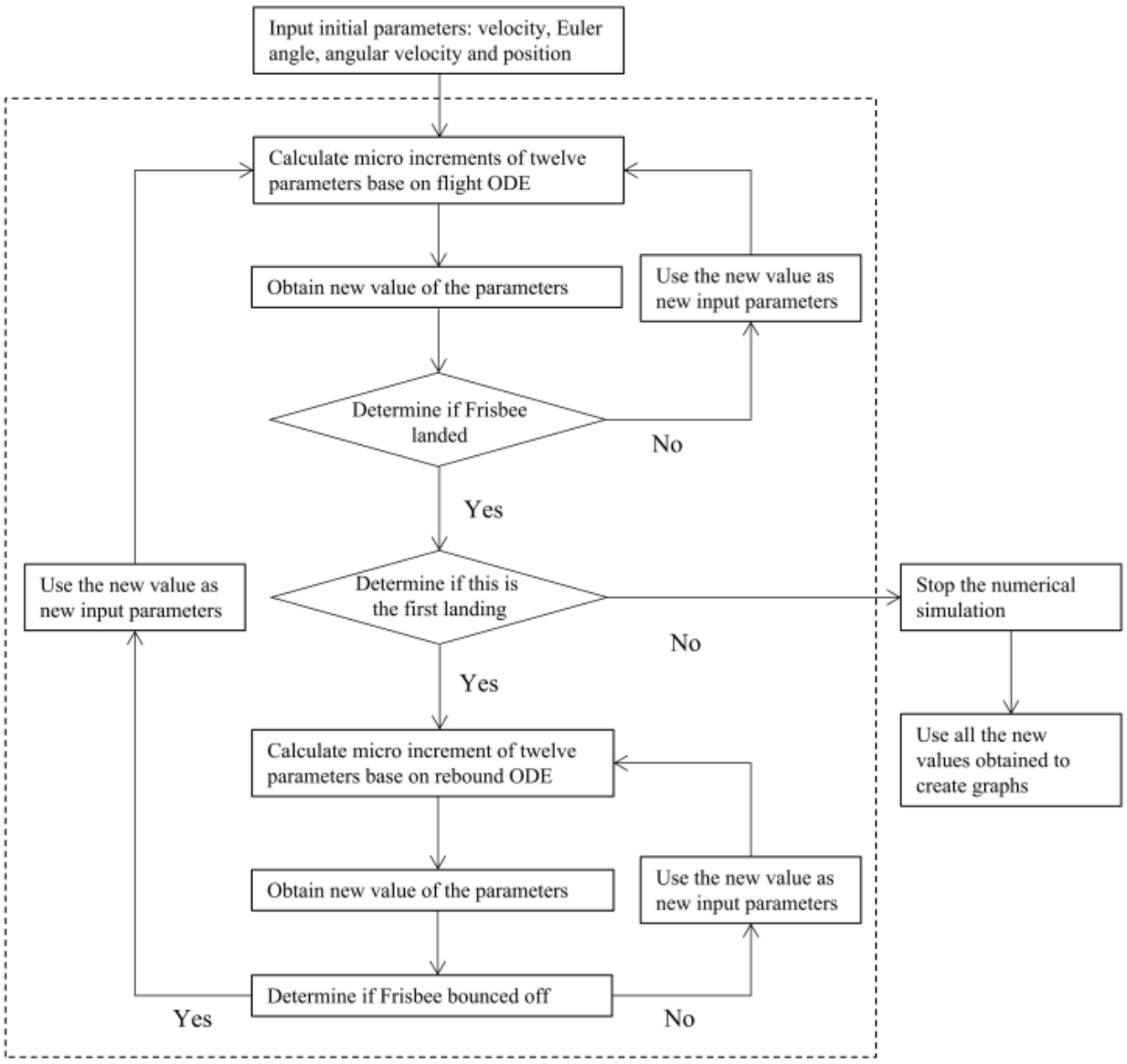


**Figure 5.** Flowchart for the numerical simulation of Frisbee dynamics.

### 4.2. Simulation of typical Frisbee flight path including rebound

In 1999, Kunio Yasuda measured the range of initial parameters for free Frisbee flights using camara sets. As indicated by analysis of the videos recorded, Yasuda determined that the most typical initial velocity, angular velocity and attack angle of Frisbee flight. A typical initial velocity is $10-10.5m/s$; a typical initial angular velocity is $350-450rpm$, which is about $37-47rad/s$; a typical attack angle is 10°, which is about $0.175rad$ [12]. The initial launching height is arbitrarily set at $1m$, congruent with the height of human's hand. A pitch angle of $0.275rad$ is set. This indicates a $0.1rad$ angle make between the initial velocity and the ground, and can simulate the scenario that the Frisbee is thrown up into the air. Therefore, from these initial parameters, setting an accuracy at $1.0E-5$, the following graphs are the results from simulation, with different initial parameter sets labeled in the graph title. Eight initial parameter sets are presented. The spring constant and damping coefficient is set using the experiment result in section 5.

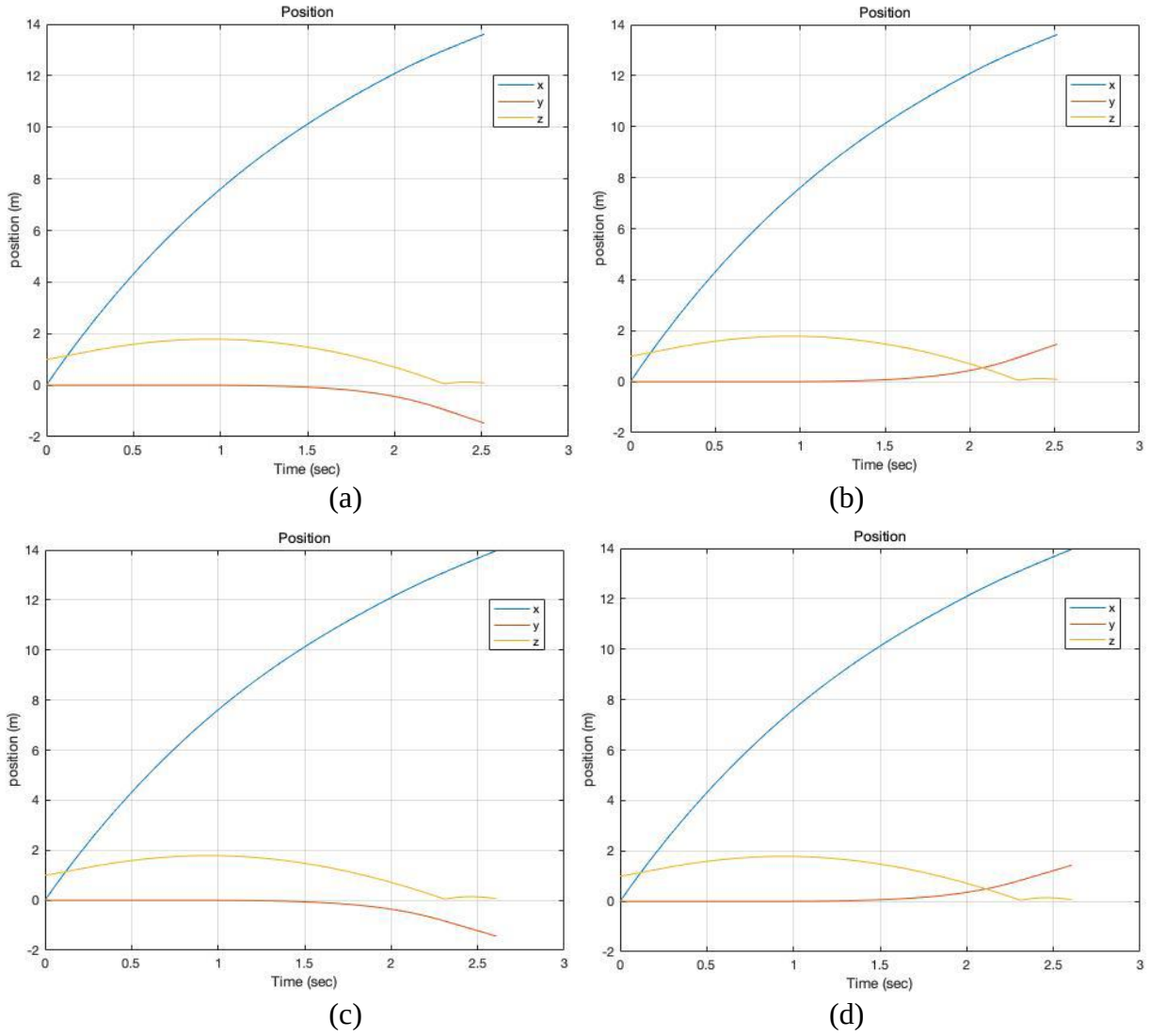


**Figure 6.** Position $x$, $y$, and $x$ of Frisbee with different initial velocity, angular velocity an(a):10$m/s$, 37$rad/s$, 0.175$rad$ attack angle, 0.275$rad$ pitch angle, 1m initial height; (b):10$m/s$, −37$rad/s$, 0.175$rad$ attack angle, 0.275$rad$ pitch angle, 1$m$ initial height; (c):10$m/s$, 40$rad/s$, 0.2$rad$ head-up position; (d):10$m/s$, −40$rad/s$, 0.2$rad$ head-up position

### 4.3. Simulation of rebound pattern

Typically, to achieve the degree of rebound author observed when engaging in Frisbee class, the Frisbee would have to be launched toward the ground. This way, the force exerted by the ground would be enough to invert the vertical velocity of Frisbee and adjust Frisbee's attitude, so that the lift generated would be enough to continue climbing up high. Typically, Frisbee won't fly up too high in rebound. However, if a large force is applied to throw the Frisbee, giving the Frisbee a large initial velocity, Frisbee could climb up high during rebound. By setting the initial parameters to be 13$m/s$, -60$rad/s$, 0.1$rad$ attack angle, -0.1$rad$ pitch angle, and 0.1$m$ from the ground, one typical rebound process (Frisbee do not fly up high) is established. The change in position, velocity, angular velocity and Euler angle for this high rebound is presented in Figure 7. Additionally, By setting the initial parameters to be 15$m/s$, 60$rad/s$, 0.2$rad$ attack angle, -0.1$rad$ pitch angle, and 0.1$m$ from the ground, one rebound process involving Frisbee climbing up high is established. The change in position, velocity, angular velocity and Euler angle for this high rebound is presented in Figure 8.

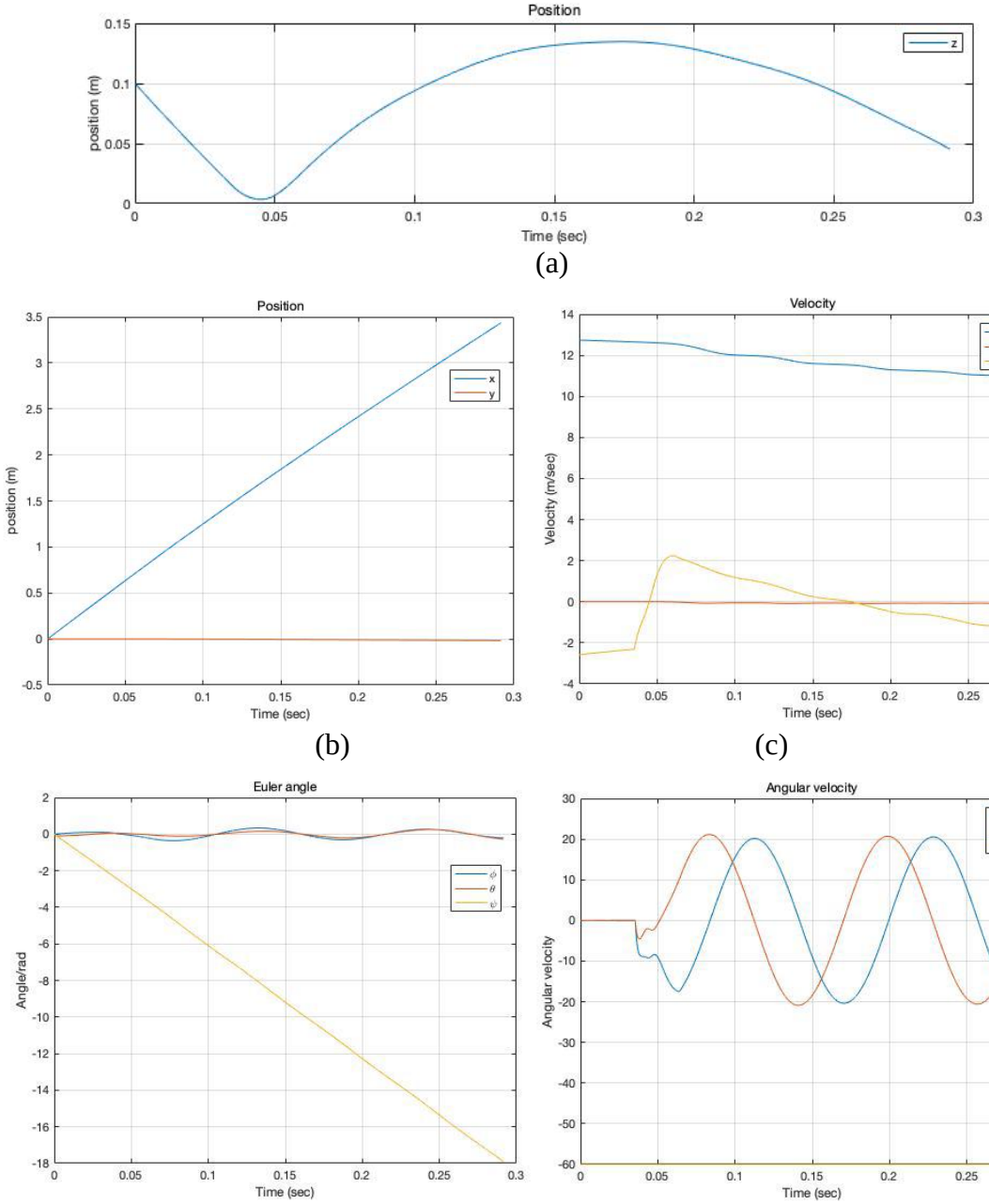


**Figure 7.** Initial parameters: position (0, 0, -0.1), velocity (13·cos(-0.2), 0, -15·sin(-0.2)), angular velocity (0, 0, -60), Euler angle (0, -0.1, 0); (a): $z$ position of Frisbee during rebound process; (b):$x$ and $y$ position of Frisbee during rebound process; (c):velocity of Frisbee during rebound process; (d): Euler angle of Frisbee during rebound process; (e): angular velocity of Frisbee during rebound process

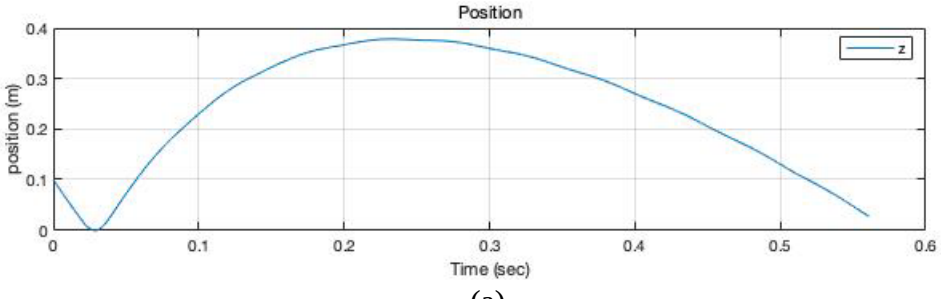

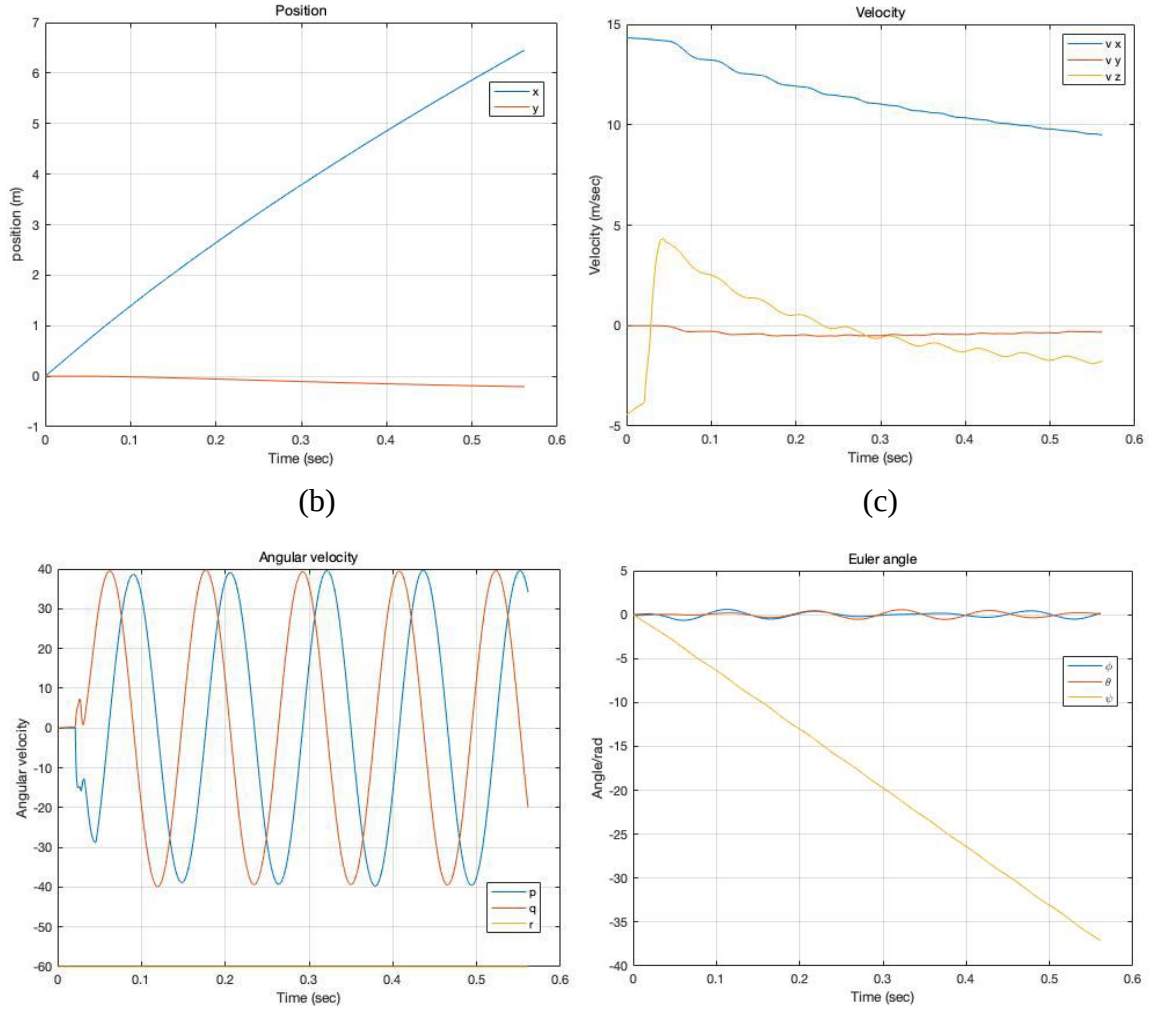


**Figure 8.** Initial parameters: position (0, 0, -0.1), velocity (15·cos(-0.3), 0, -15·sin(-0.3)), angular velocity (0, 0, -60), Euler angle (0, -0.1, 0); (a): $z$ position of Frisbee during rebound process; (b):$x$ and $y$ position of Frisbee during rebound process; (c):velocity of Frisbee during rebound process; (d): Euler angle of Frisbee during rebound process; (e): angular velocity of Frisbee during rebound process

A clear pattern could be seeing in these five graphs, the rebound phenomenon on vertical direction could be identified. The impact caused an intense change in Frisbee's attitude, result in drastic fluctuation of the two components of the angular velocity $p$ and $q$. The vertical velocity has the direction shifted in a sudden, signaling the impact, and the noticeable fluctuation of the vertical velocity after rebound could be a result of the drastically fluctuating angular velocity.

## 5. Motion of Frisbee before and after touching down

### 5.1. Setup

In this section, an experiment is conducted using equipment to record the motion of Frisbee in air and after touch down on a plastic pad. The Frisbee is launched with different linear velocity, angular velocity and initial attitude by a specifically made Frisbee launcher. Frisbee's initial spin rate and pitch angle could be adjusted by the launcher.

To record the motion of the Frisbee, two cameras were set. The first one recording Frisbee's motion along $x$ and $z$ direction was put on the side of the experiment set up, perpendicular to Frisbee's trajectory. The second one recording Frisbee's motion along $y$ direction was put in front of the

experiment set up, parallel to Frisbee's trajectory. In order to amplify the phenomenon of rebound, and to create an experiment condition closer to the assumptions of the theoretical model, rubber plastic pads were used for Frisbee to land on and rebound after touching down. The spring constant and damping coefficient of the pads are determined by experiment to be 13774 and 32.676 respectively.

### 5.2. Experiment procedure

8 different set of initial parameters were be tested in the experiment. The pitching angle of the launching plane is set using an electronic level, which can give the exact value of degree. Using the level, the pitch of the plane could be set at the required experiment condition. After having the pads placed properly, set the two cameras at their location. Turn on the Frisbee Launcher and start recording videos, put the five identical Frisbee, which have rotational inertia around x y and z axis determined using three wire pendulum to be 0.0012kg/m$^2$, 0.0012kg/m$^2$, and 0.0023kg/m$^2$ respectively, in the launcher one by one and launch the Frisbee. Keep repeating the experiment until there are in total 3 trials each initial parameter that the Frisbee lands on the pad, since in some cases, due to influence of uncontrollable factors such as wind, Frisbee lands on asphalt ground rather then on plastic pad.

### 5.3. Video analysis

The videos recorded for the experiment are imported in tracker for analysis. Manually track Frisbee's trajectory in the series of images by import a point in tracker and click to track the center of Frisbee in each frame. In each set of experiment, 6 videos are recorded for the three trials. The position of Frisbee in $y$ direction is a bit more complicated. In more common cases, the camera is somewhat slightly off the course of the Frisbee, and cause an angle between its vision and Frisbee's initial trajectory. This situation is in essence the same as if Frisbee is launched with an initial velocity along $y$ direction. Therefore, when analyzing the position along $y$ direction, the velocity on $y$ direction is also obtained to supply the initial parameters.

The velocity and the angular velocity are then put in MATLAB source code to obtain the position of Frisbee predicted by the theoretical calculation as a function of time. The accuracy for the simulation is set to be 1.0E−5. Data presented in the following sections, organized by initial parameter. The negativity of $y$ obtained in Tracker is opposite to previous definition because of Tracker's default setting. Therefore, the $y$ position is invert in negativity when using MATLAB to create graphs.

#### 5.3.1 Speed 1 (8m/s), 7 degree pitch, 52cm above ground

Speed 1 is determined by tracker analysis to be $8m/s$. The $x$ and $z$ position as a function of time is presented in Figure 9.

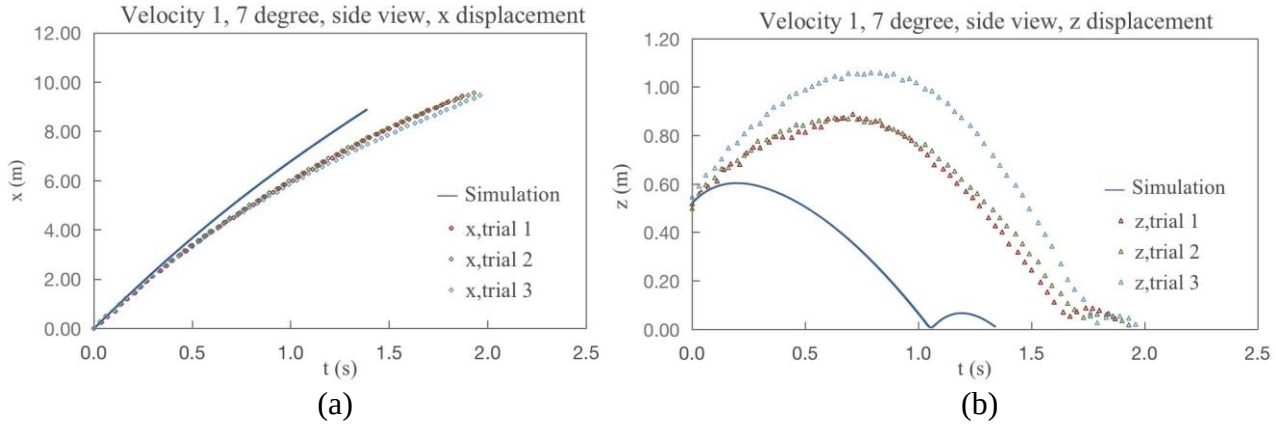


(a) (b)

**Figure 9.** (a) $x$ displacement and (b) $z$ displacement. The initial condition for this set of experiment and simulation has speed $8m/s$, pitch angle of 7°, and height of $52cm$ above ground. The solid line is obtained from simulation and the markers are three trials obtained from experiments.

The initial velocity along $y$ direction is determined to be about $0.05m/s$. The $y$ position as a function of time is presented in Figure 10.

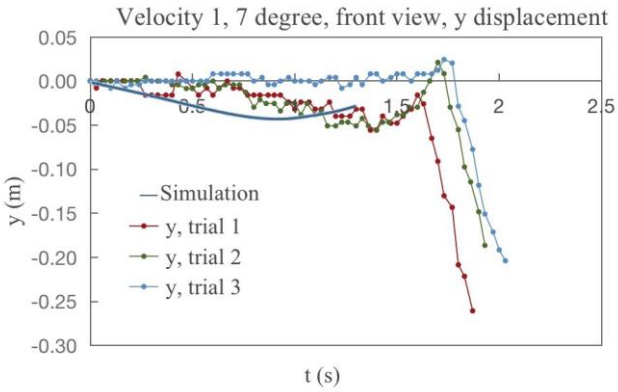


**Figure 10.** $y$ displacement, $y$ component of speed $0.05m/s$

### 5.3.2 Speed 1 (8m/s), 14 degree pitch, 61cm above ground

The $x$ and $z$ position as a function of time is presented in Figure 11.

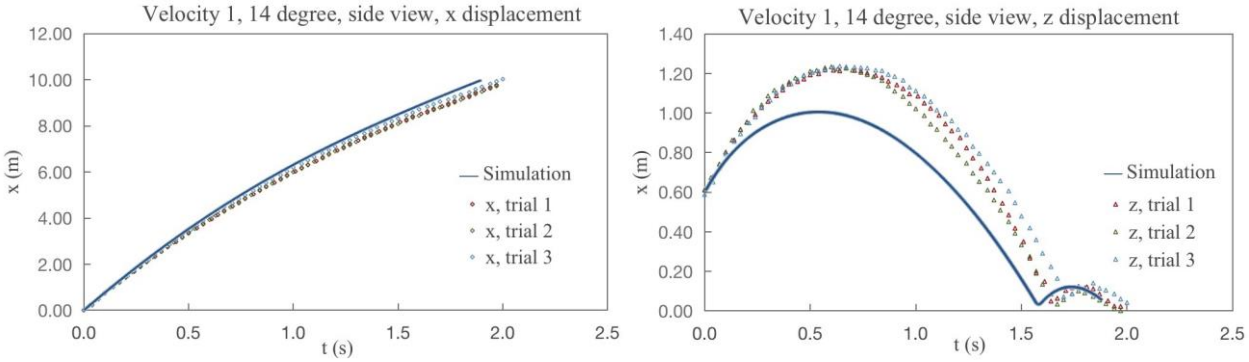


(a) (b)

**Figure 11.** (a) $x$ displacement and (b) $z$ displacement. The initial condition for this set of experiment and simulation has speed $8m/s$, pitch angle of 14°, and height of $61cm$ above ground. The solid line is obtained from simulation and the markers are three trials obtained from experiments.

The initial velocity along $y$ direction is determined to be about $0.1m/s$. The $y$ position as a function of time is presented in Figure 12.

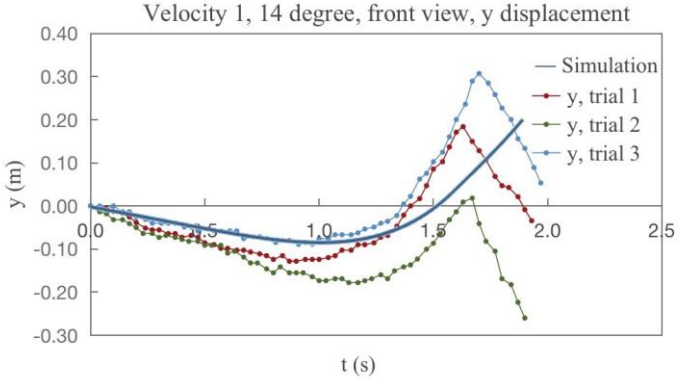


**Figure 12.** $y$ displacement, $y$ component of speed $0.1m/s$

### 5.3.3 Speed 2 (8.5m/s), 7 degree pitch, 52cm above ground

Speed 2 is determined to be $8.5m/s$. The $x$ and $z$ position as a function of time is presented in Figure 13.

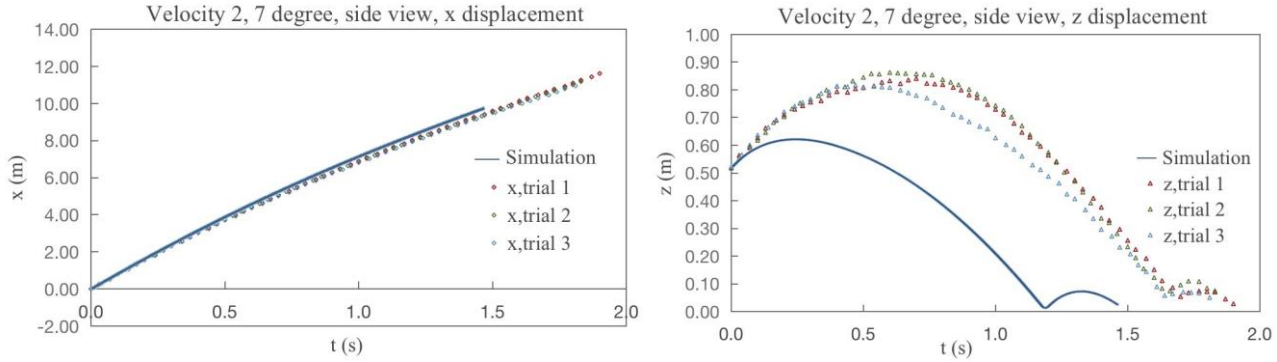


(a) (b)

**Figure 13.** (a) $x$ displacement and (b) $z$ displacement. The initial condition for this set of experiment and simulation has speed 8.5$m/s$, pitch angle of 7°, and height of 52$cm$ above ground. The solid line is obtained from simulation and the markers are three trials obtained from experiments.

The initial velocity along $y$ direction is determined to be about -0.15$m/s$. The $y$ position as a function of time is presented in Figure 14.

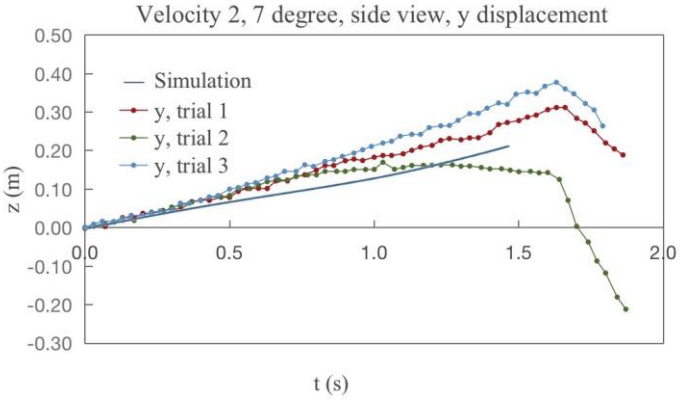


**Figure 14.** $y$ displacement, $y$ component of speed -0.15$m/s$

### 5.3.4 Speed 2 (8.5m/s), 14 degree pitch, 61cm above ground

The $x$ and $z$ position as a function of time is presented in Figure 15.

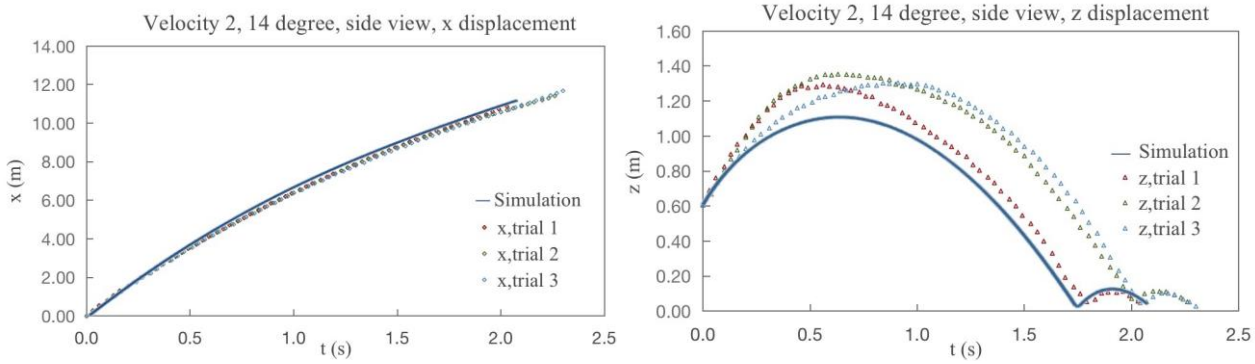


(a) (b)

**Figure 15.** (a) $x$ displacement and (b) $z$ displacement. The initial condition for this set of experiment and simulation has speed 8.5$m/s$, pitch angle of 14°, and height of 61$cm$ above ground. The solid line is obtained from simulation and the markers are three trials obtained from experiments.

The initial velocity along $y$ direction is determined to be about -0.1$m/s$. The $y$ position as a function of time is presented in Figure 16.

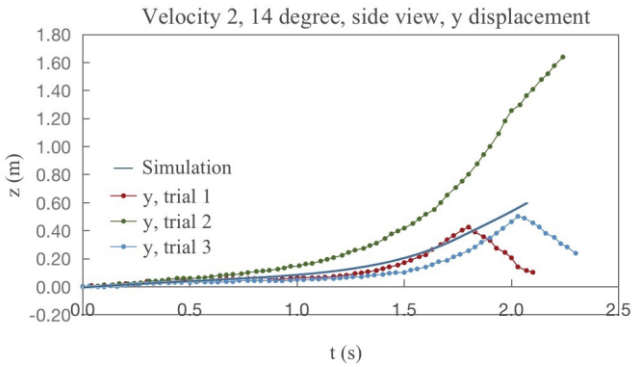


**Figure 16.** $y$ displacement, $y$ component of speed -0.1$m/s$

### 5.3.5 Speed 3 (9m/s), 7 degree pitch, 52cm above ground

Speed 3 is determined to be 9$m/s$. The $x$ and $z$ position as a function of time is presented in Figure 17.

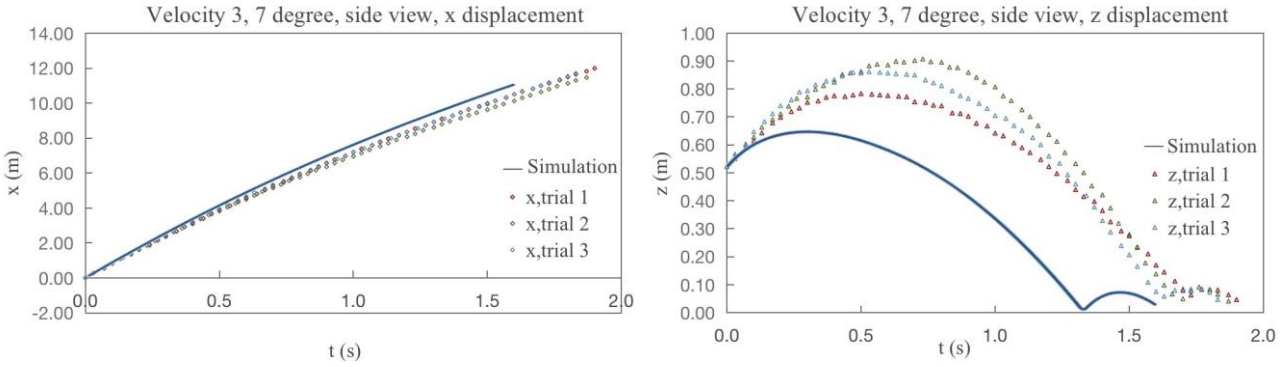


(a) (b)

**Figure 17.** (a) $x$ displacement and (b) $z$ displacement. The initial condition for this set of experiment and simulation has speed 9$m/s$, pitch angle of 7°, and height of 52$cm$ above ground. The solid line is obtained from simulation and the markers are three trials obtained from experiments.

The initial velocity along $y$ direction is determined to be about -0.3$m/s$. The $y$ position as a function of time is presented in Figure 18.

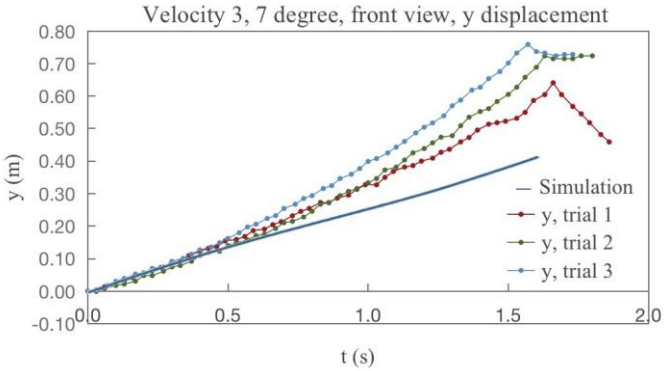


**Figure 18.** $y$ displacement, $y$ component of speed -0.3$m/s$

### 5.3.6 Speed 3 (9m/s), 14 degree pitch, 61cm above ground

The $x$ and $z$ position as a function of time is presented in Figure 19.

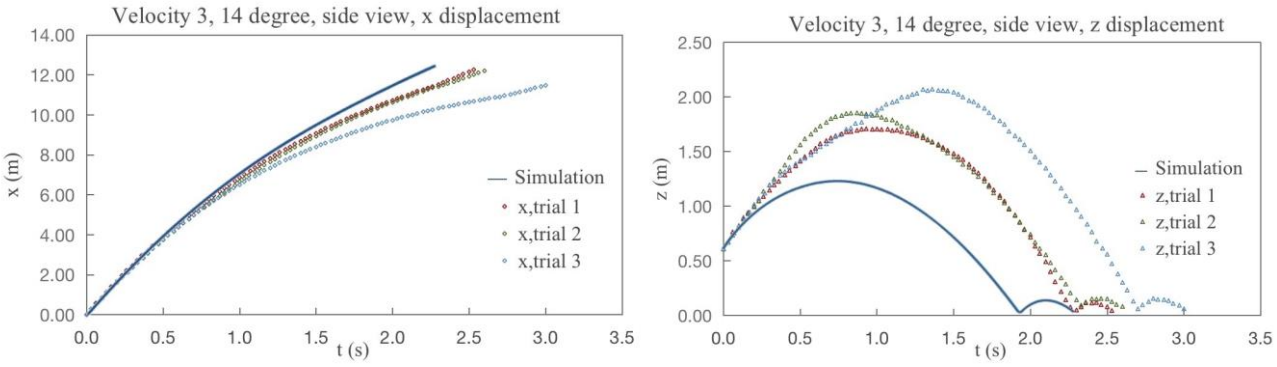


(a) (b)

**Figure 19.** (a) $x$ displacement and (b) $z$ displacement. The initial condition for this set of experiment and simulation has speed $9m/s$, pitch angle of 14°, and height of $61cm$ above ground. The solid line is obtained from simulation and the markers are three trials obtained from experiments.

The initial velocity along $y$ direction is determined to be about -0.2$m/s$. The $y$ position as a function of time is presented in Figure 20.

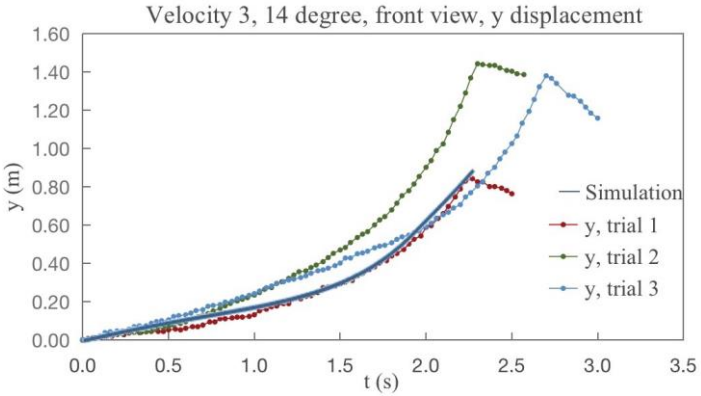


**Figure 20.** $y$ displacement, $y$ component of speed -0.2$m/s$

### 5.3.7 Speed 4 (9.5m/s), 7 degree pitch, 52cm above ground

Speed 4 is determined to be 9.5$m/s$. The $x$ and $z$ position as a function of time is presented in Figure 21.

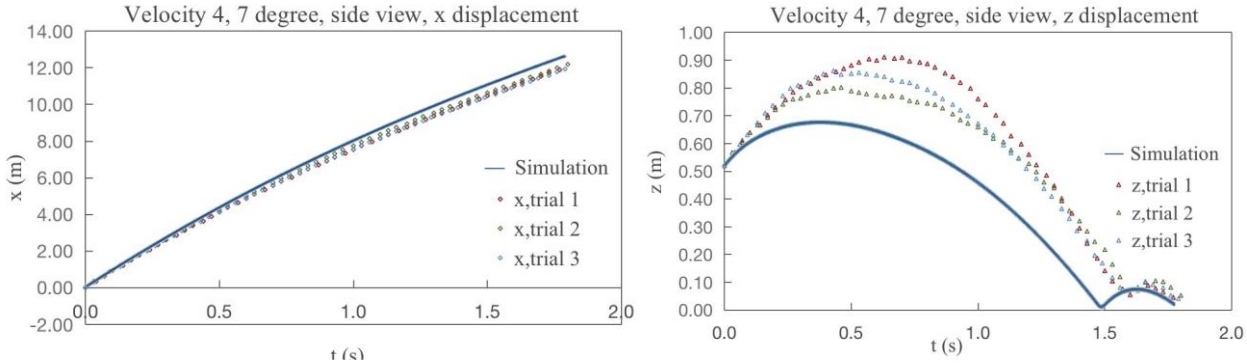


(a) (b)

**Figure 21.** (a) $x$ displacement and (b) $z$ displacement. The initial condition for this set of experiment and simulation has speed 9.5$m/s$, pitch angle of 7°, and height of 52$cm$ above ground. The solid line is obtained from simulation and the markers are three trials obtained from experiments.

The initial velocity along $y$ direction is determined to be -0.1$m/s$. The $y$ position as a function of time is presented in Figure 22.

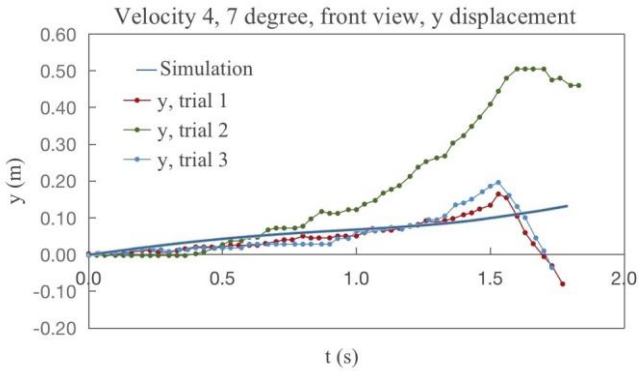


**Figure 22.** $y$ displacement, $y$ component of speed -0.1$m/s$

### 5.3.8 Speed 4 (9.5m/s), 14 degree pitch, 61cm above ground

The $x$ and $z$ position as a function of time is presented in Figure 23.

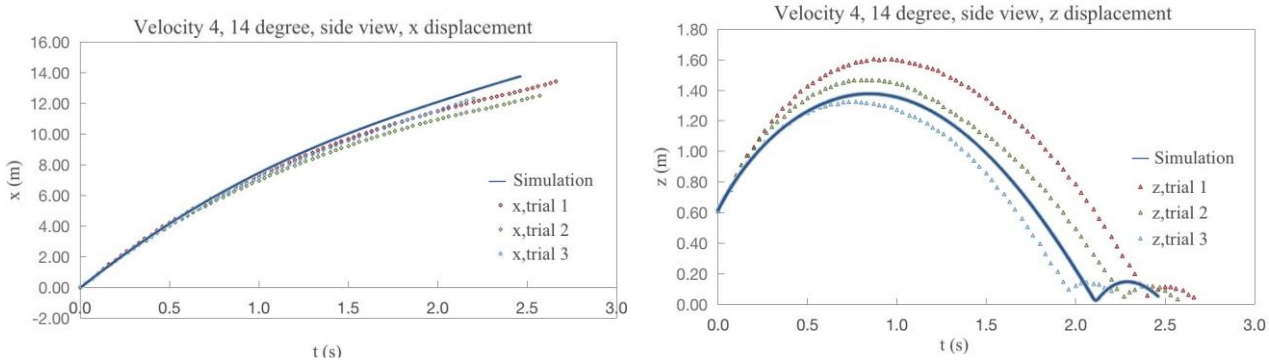


(a) (b)

**Figure 23.** (a) $x$ displacement and (b) $z$ displacement. The initial condition for this set of experiment and simulation has speed 9.5$m/s$, pitch angle of 14°, and height of 61$cm$ above ground. The solid line is obtained from simulation and the markers are three trials obtained from experiments.

The initial velocity along $y$ direction is determined to be about 0$m/s$. Additionally, Frisbee launched in this group is observed to have a 1 degree row angle. The $y$ position as a function of time is presented in Figure 24.

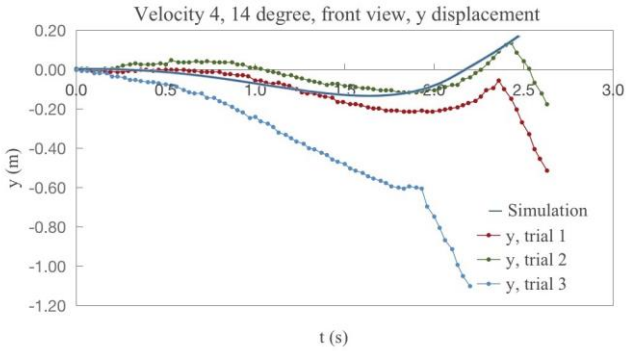


**Figure 24.** $y$ displacement, $y$ component of speed 0$m/s$ (Frisbees launched in this set of experiment has an initial row angle of about 1 degree)

### 5.4. Data Analysis and Error analysis

Based on the Figures 9-24 in the previous part, the simulation result is consistent with the experimental measurements of actual flight and rebound trajectory. In particular, the simulated $x$ and $y$ position of Frisbee match the data obtained in experiments well. The measured $y$ position changes drastically during the rebound. However, this pattern is not seeing on the theoretical model. This is

because that the theoretical model used in this research has been simplified with friction force ignored. Although the friction of rubber plastic pad is significantly smaller then asphalt pavement, and the impact time is very short, because the instantaneous impulse is quite large, the normal force exerted on Frisbee is significant during rebound, and so is the friction. The complete version of the theoretical model suggested in section 3, which takes friction into account, should be able to recreate this special pattern.

There is, however, visible discrepancy between the simulated $z$ position of Frisbee and the measured $z$ position of Frisbee, especially seen clearly in Figure 9(b), Figure 13(b), Figure 17(b) and Figure 19(b). This visible discrepancy is resulted under the influence of the wind. As recorded by an anemometer, The wind speed during the experiment is about between 0-2$m/s$, blowing against the direction of motion of Frisbee. The wind speed is not that high, however, because Frisbee's motion relies largely on the aerodynamic force, and that Frisbee does not fly at a high speed, going at a ground speed of 10$m/s$ plus wind speed of 2$m/s$ will give an air speed of 12$m/s$. Therefore, the wind, no matter how small, always has a significant effect on altering Frisbee's motion in air. This is also supported by the experiment data. With wind blowing against the motion of Frisbee, the drag will be larger. This will result in Frisbee decelerating faster than as suggested in the theoretical model. The larger deceleration could be seen in almost all the $xvs.t$ graph. Additionally, with a higher air speed, the lift force will also be larger, and could support the Frisbee to fly higher, consistent with the pattern presented in the $z$-$t$ graph.

To better avoid the influence of wind, Frisbee experiment will need to be conducted indoor. Yet, despite of all the influence Frisbee experienced during experiment (wind, friction and such), the simulated result matches the experiment data. The simulated vertical motion of Frisbee during and after rebound is highly similar to the result obtained by experiment, indicating that the "damping spring" model of rebound successfully describes Frisbee's rebound phenomenon.

## 6. Conclusions and future work

### 6.1. Conclusion

This paper is the first one to investigate the touchdown dynamics of the Frisbee to the best of the author's knowledge. Dynamic differential equations of Frisbee flight have been established based on previous works with improvements, where moments and forces are unified into the same reference frame through vector transformation. Velocity of Frisbee is computed in the inertial Frame to provide better clearance and to support the deduction of rebound model, which is developed based on rigid body dynamics. The ground is modeled as a damping spring. Governing equations are then developed to calculate the damping coefficient and spring constant of the ground using experiment data. Dynamic differential equations of rebound are developed taking the friction and normal force into account, while the final model presented here is simplified by neglecting the friction for brevity.

MATLAB simulation for the equations governing flight and the simplified equations governing rebound is developed using ODE23s solver. The aerodynamic coefficients are based on database from existing experiments. Comparison between simulation result of velocity in inertial frame and in embedded frame illustrates the advantage of calculating velocity in inertial frame. Simulations for the typical Frisbee flight trajectories are done with the same initial parameters as these in previous work. Simulation results for two different rebound processes are also provided.

Experiments are conducted to validate the numerical simulation. The moment of inertia through horizontal axis and vertical axis for a specific Frisbee with known basic parameter is determined using the three wire pendulum method. Damping coefficient and spring constant of a rubber plastic pad is determined by video analysis following equations deducted. Identical Frisbees are then launched by a launcher for three times and the motion is recorded by a camera. Totally eight different initial parameter sets are tested in the experiment. A frame by frame analysis of recorded flight videos is done to get the position and velocity of Frisbee as a function of time. The comparison between experimental measurements and numerical simulation results of respective initial parameters

demonstrate that the model established captures the influence of aerodynamic forces, aerodynamic torques and self spinning of Frisbee on its flight and rebound pattern.

### 6.2. Future works

This work opens up many promising future work direction, where primary direction is to simulate the rebound of Frisbee base on the complete rebound theory by adding in the friction. Because of the complexity of the equation, this will require better computational capacity. Simulation result of the complete rebound theory should give a more precise rebound pattern by taking friction into account. Another follow up work that could be carry on is to repeat the experiments indoor to avoid the influence of wind. This should provide a better look at the original trajectory of Frisbee flight and rebound. The influence of wind could also be added into the numerical simulation as a modification term. This could give a more accurate result of Frisbee's motion under windy condition, and could be used in the development of a similar UAV.

Last but not the least, the launching strategy of Frisbee could be studied by run the MATLAB program in cycle. As an example, combination of parameters lead to a smooth landing could be studied. When Frisbee touchdown with perfect or near perfect horizontal attitude, the concaved bottom side of Frisbee would create an air cushion that buffers the impact. With the air cushion lifting the Frisbee, it normally would land smoothly without having any rebound.

## References

[1] Bloomfield L A. The flight of the frisbee. Scientific American, 280(4):132–132, 1999.

[2] Wie B. Space vehicle dynamics and control. Aiaa, 1998.

[3] Stilley G D Carstens D L. Adaptation of the frisbee flight principle to delivery of special ordnance. In 2nd Atmospheric Flight Mechanics Conference, page 982, 1972.

[4] Potts J R Crowther W J. Frisbee (TM) aerodynamics. In 20th AIAA applied aerodynamics conference, page 3150, 2002.

[5] Lorenz R D. Spinning Flight: Dynamics of Frisbees, Boomerangs, Samaras, and Skipping Stones. Springer, 2006.

[6] Miller I A Giancoli D C. Physics: principles with applications. Prentice Hall Upper Saddle River, NJ, USA:, 1998.

[7] Nagahiro S Hayakawa Y. Theoretical and numerical approach to "magic angle" of stone skipping. Physical review letters, 94(17):174501, 2005.

[8] Clanet C Hersen F, Bocquet L. Secrets of successful stone-skipping. Nature, 427(6969):29–29, 2004.

[9] Hubbard M Hummel S. Identification of Frisbee aerodynamic coefficients using flight data. volume 20, 2002.

[10] Hubbard M Hummel S A. Simulation of Frisbee flight. 5th Conference on Mathematics and Computers in Sport, University of Technology, Sydney, pages 124–134, 2000.

[11] Baumback K. The aerodynamics of frisbee flight. Undergraduate Journal of Mathematical Modeling, 2010.

[12] Yasuda K. Flight and aerodynamic characteristics of a flying disk. Japanese Soc. Aero. Space Sci, 47(547):16–22, 1999.

[13] Kamaruddin N M. Dynamics and performance of flying discs. The University of Manchester (United Kingdom), 2011.

[14] Landell-Mills N. Newtons laws explain how Frisbees fly. European Journal of Applied Physics, 2(4), 2020.

[15] Crowther W J Potts J R. Simulation of a spinstabilised sports disc. Sports Engineering, 10(1):3–21, 2007.

[16] Morrison V R. The physics of Frisbees. Electronic Journal of Classical Mechanics and Relativity, 8(48), 2005.

[17] Sharma S Siddiqui Y, et. al. Design and manufacturing of Frisbee launching robot. International Journal of Current Engineering and Technology, 2017.

[18] Weizman Y Tan A M. Measurement of flight dynamics of a frisbee using a triaxial mems gyroscope. 49(1): 66, 2020.

[19] Mosca G Tipler P A. Physics for scientists and engineers. Macmillan, 2007.

[20] Beard R W. Quadrotor dynamics and control. Brigham Young University, 19(3): 46–56, 2008.